Phonon Anharmonicities in Graphite and Graphene

Nicola Bonini,[1] Michele Lazzeri,[2] Nicola Marzari,[1] and Francesco Mauri[2]

[1]*Department of Materials Science and Engineering, Massachusetts Institute of Technology, Cambridge Massachusetts 02139, USA*
[2]*IMPMC, Universités Paris 6 et 7, CNRS, IPGP, 140 rue de Lourmel, 75015 Paris, France*

(Received 7 April 2007; published 24 October 2007)

We determine from first principles the finite-temperature properties—linewidths, line shifts, and lifetimes—of the key vibrational modes that dominate inelastic losses in graphitic materials. In graphite, the phonon linewidth of the Raman-active E_{2g} mode is found to decrease with temperature; such anomalous behavior is driven entirely by electron-phonon interactions, and does not appear in the nearly degenerate infrared-active E_{1u} mode. In graphene, the phonon anharmonic lifetimes and decay channels of the A_1' mode at K dominate over E_{2g} at Γ and couple strongly with acoustic phonons, highlighting how ballistic transport in carbon-based interconnects requires careful engineering of phonon decays and thermalization.

DOI: 10.1103/PhysRevLett.99.176802 PACS numbers: 73.22.−f, 71.15.Mb, 78.30.Na, 81.05.Uw

Carbon nanotubes and graphene nanoribbons are intensely studied as candidates for future electronic and optoelectronic devices. In particular, metallic tubes have some of the highest current densities reported in any material [1] and could lead to extremely promising applications as electrical interconnects. However, in carbon nanotubes or graphite, high currents [2–4] or optical excitations [5,6] can induce a nonthermal phonon distribution, with significant overpopulation of the optical phonons E_{2g} at Γ and A_1' at K. These *hot phonons* develop because of a slower anharmonic decay rate with respect to the generation rate [4], and cause a significant reduction of the ballistic conductance of carbon nanotubes at bias potentials larger than $\sim$0.2 V, severely limiting interconnect performance [1–4]. A microscopic characterization of phonon decays [7] is thus a key step in improving the transport properties of these materials, whereas engineering individual decay channels would allow to control energy relaxation and ultimately performance.

Information on the phonon scattering mechanisms can be obtained from Raman or infrared (IR) measurements of the linewidths and line shifts of the phonon modes [8]. Indeed, the intrinsic linewidth γ^{in} in a defect-free sample is $\gamma^{\text{in}} = \gamma^{e\text{-ph}} + \gamma^{\text{ph-ph}}$, where $\gamma^{e\text{-ph}}$ and $\gamma^{\text{ph-ph}}$ represent the electron-phonon (e-ph) and anharmonic phonon-phonon (ph-ph) interactions [9,10]. The shift with temperature of the harmonic phonon frequencies is also due to ph-ph interactions [8,11,12]. While experimental measurements are now available on graphene, graphite, and carbon nanotubes, their interpretation is not always straightforward. For example, graphene has a E_{2g} at Γ Raman-active mode (the G band) with a linewidth of $\sim$13 cm^{-1} [13]. In graphite this phonon splits in two nearly degenerate modes: the Raman-active E_{2g} and the IR-active E_{1u} [14]. The linewidth of the Raman-active mode (11.5 cm^{-1} [15]) remains similar to that of graphene, suggesting a negligible effect of the interactions among different graphitic planes. On the other hand, IR measurements show that the linewidth of the E_{1u} mode is much smaller ($\sim$4 cm^{-1} [14]). The finite-temperature line shift of E_{2g} is also puzzling: recent experimental results have shown very little difference between graphite and graphene [16], while first-principles calculations find a room-temperature in-plane thermal-expansion coefficient for graphene more than 3 times as large as that of graphite (both are negative) [17]. Prompted by these results, and by the central role played by phonon decays in controlling inelastic losses, we characterize here the e-ph and ph-ph scattering parameters of the E_{2g}, E_{1u}, and A_1' modes in graphite or graphene using state-of-the-art first-principles calculations. These parameters are then used to compute the linewidths and line shifts of the Raman and IR bands, and the ph-ph decay lifetimes.

All the calculations are performed using density-functional theory (DFT) and density-functional perturbation theory (DFPT) [18] as implemented in the PWSCF package of the QUANTUM-ESPRESSO distribution [19]. We use the local-density approximation [20], norm-conserving pseudopotentials [21], and a plane-wave expansion up to a 55 Ry cutoff. Brillouin-zone sampling is performed on $32 \times 32 \times 8$ and $32 \times 32 \times 1$ Monkhorst-Pack meshes for graphite and graphene, with a Fermi-Dirac smearing in the electronic occupations of 0.02 Ry. For graphite, the equilibrium lattice parameters $a = 2.43$ Å and $c/a = 2.725$ are used [17]; for graphene, an interlayer spacing of 7 Å is adopted. The DFT accuracy in calculating vibrational properties in graphite even in the presence of van der Waals interactions is discussed in Ref. [17]. The phonon frequencies, dynamical matrices, and e-ph matrix elements are obtained using DFPT. The phonon anharmonic self-energy is given, at the lowest order in the perturbative expansion with respect to the atomic mass, by the tadpole, loop, and bubble diagrams [22] corresponding to three- and four-phonon scattering terms. Thus, we calculate the third- and fourth-order derivatives of the total energy with respect to atomic displacements; the former are obtained from DFPT [18,23], while the latter from

finite differences over the relevant phonon eigenvectors. The dynamical matrices are computed on a $16 \times 16 \times 1$ or a $8 \times 8 \times 4$ mesh (for graphene and graphite, respectively), higher-order derivatives on $4 \times 4 \times 1$ or $4 \times 4 \times 2$ meshes. Fourier interpolation [18] then provides all these quantities on finer grids ($200 \times 200 \times 50$ and $200 \times 200 \times 1$ for graphite and graphene), over which we perform all numerical integrations.

At the lowest order, a phonon acquires a finite linewidth by decaying into two lower-energy phonons ($\gamma^{\text{ph-ph}}$) or by creating an electron-hole pair ($\gamma^{e\text{-ph}}$). The ph-ph contribution $\gamma^{\text{ph-ph}}$ is given by the imaginary part of the phonon self-energy Π [8,22], which is determined by 3-phonon scattering processes. In the electron-hole creation process, a phonon with wave vector $\mathbf{q}$ excites an electronic state $|\mathbf{k}i\rangle$ with wave vector $\mathbf{k}$ into the state $|(\mathbf{k}+\mathbf{q})j\rangle$. The scattering probability is thus given by the e-ph coupling matrix element $g_{(\mathbf{k}+\mathbf{q})j,\mathbf{k}i}$ [24]. According to the Fermi golden rule [25]

$$\gamma_{\mathbf{q}}^{e\text{-ph}}(T) = \frac{4\pi}{N_k} \sum_{\mathbf{k},i,j} |g_{(\mathbf{k}+\mathbf{q})j,\mathbf{k}i}|^2 [f_{\mathbf{k}i}(T) - f_{(\mathbf{k}+\mathbf{q})j}(T)] \times \delta[\epsilon_{\mathbf{k}i} - \epsilon_{(\mathbf{k}+\mathbf{q})j} + \hbar\omega_{\mathbf{q}}], \quad (1)$$

where $\omega_{\mathbf{q}}$ is the phonon frequency, the sum is on N_k $\mathbf{k}$ vectors, $f_{\mathbf{k}i}(T)$ is the Fermi-Dirac occupation at temperature T for an electron with energy $\epsilon_{\mathbf{k}i}$, and δ is the Dirac delta [26] [throughout the Letter we will consider full width at half maximum (FWHM) linewidths].

We report in Fig. 1 the linewidths for the E_{2g} and E_{1u} modes in graphite and graphene, computed according to the aforementioned procedure. Very good agreement is found with respect to measurements [13–15]. More importantly, our calculations show that the phonon linewidth for the E_{2g} mode, and its dependence on temperature, is completely dominated by the e-ph coupling, with a *decreasing linewidth as a function of temperature*. This effect is due to the strong T dependence of $\gamma^{e\text{-ph}}$, which is only partially compensated by $\gamma^{\text{ph-ph}}$.

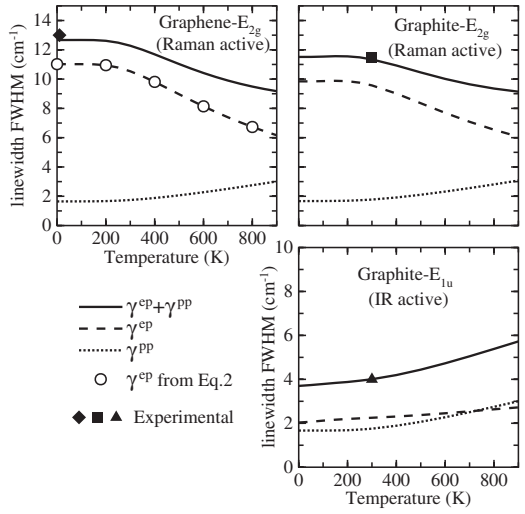

FIG. 1. Total linewidths (solid line) for the E_{2g} and E_{1u} modes in graphene and graphite and their e-ph ($\gamma^{e\text{-ph}}$, dashed line) and ph-ph ($\gamma^{\text{ph-ph}}$, dotted line) contributions, together with the results of Eq. (2) (circles). Measurements from Refs. [13–15].

In order to rationalize this result, we consider a simplified model for the temperature dependence of $\gamma^{e\text{-ph}}$ for the E_{2g} modes: we assume a linearized band dispersion around the Fermi energy (ϵ_F) and a model e-ph coupling [24]. It can be easily shown (e.g., following Eq. 3 in Ref. [15]) that at finite T

$$\gamma^{e\text{-ph}}(T) = \gamma^{e\text{-ph}}(0)\left[f\left(-\frac{\hbar\omega_0}{2k_BT}\right) - f\left(\frac{\hbar\omega_0}{2k_BT}\right)\right], \quad (2)$$

where, from DFT, $\gamma^{e\text{-ph}}(0) = 11.01\ \text{cm}^{-1}$ [15], $\hbar\omega_0 = 196$ meV is the E_{2g} phonon energy, k_B is the Boltzmann constant, and $f(x) = 1/[\exp(x)+1]$. Equation (2) reproduces very well the full calculation of Eq. (1) (see Fig. 1) and can be used to understand the temperature dependence of $\gamma^{e\text{-ph}}(T)$, since this is now proportional to the difference between the occupations of states below and above ϵ_F. As T increases, the occupation of filled states below ϵ_F decreases, while the empty states are occupied more, resulting in the observed decrease of $\gamma^{e\text{-ph}}(T)$ with temperature.

It is important to note that $\gamma^{e\text{-ph}}(0)$ for the E_{1u} mode in graphite is almost 5 times smaller than for the case of E_{2g}. This difference can be understood by decomposing Eq. (1) in parallel and perpendicular contributions, where $\mathbf{k}_\perp$ is the component perpendicular to the graphene planes and $\mathbf{k}_\parallel$ is the in-plane projection. We define $\gamma(k_\perp)$ as the contribution to the e-ph linewidth obtained from Eq. (1) when restricting the k-point integration on those vectors $\mathbf{k}$ that satisfy $\hat{\mathbf{c}} \cdot \mathbf{k} = k_\perp$, where $\hat{\mathbf{c}}$ is the unit vector perpendicular to the graphene planes. With such definition $\gamma^{e\text{-ph}} = \int_0^1 \gamma(k_\perp) dk_\perp$, where $k_\perp$ is in units of π/c. The electronic states with a nonzero contribution to Eq. (1) are those allowed by energy conservation and by a nonzero e-ph coupling. Energy conservation alone selects the four π bands near the Fermi level (labeled 1 to 4, from the lowest to the highest, in Fig. 2). For the E_{1u} mode the computed e-ph coupling allows mainly transitions from band 1 to 3 and from band 2 to 4. Since the minimum gap between bands 1 and 3 (and 2 and 4) varies considerably as a function of $k_\perp$, and the IR transition satisfies energy conservation only for $k_\perp \gtrsim 0.8$ (Fig. 2), we have a small $\gamma^{e\text{-ph}}$ for this mode. On the contrary, for the E_{2g} mode the e-ph coupling allows mainly transitions from band 1 to 4 and from band 2 to 3; energy-conservation means that only the transition between 2 and 3 is essentially active. Since the minimum gap between bands 2 and 3 is always zero, the transition is active for any $k_\perp$. It turns out that $\gamma_{E_{2g}}(k_\perp)$ is almost a constant and its value is similar to that of graphene (Fig. 2) and much larger than that for the IR-active mode ($\gamma_{E_{2g}}^{e\text{-ph}} \sim 5\gamma_{E_{1u}}^{e\text{-ph}}$). Interestingly, the IR-active

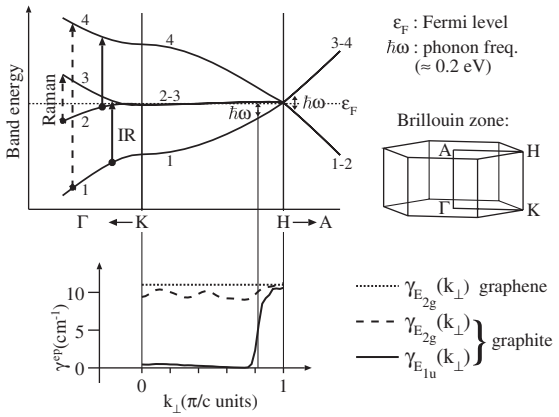

FIG. 2. e-ph coupling contributions to the linewidths ($\gamma^{e\text{-ph}}$) of the E_{2g} (Raman-active) and E_{1u} (IR-active) modes. Upper panel: the four π bands of graphite. Lower panel: Decomposition of $\gamma^{e\text{-ph}}$ into the different $k_\perp$ contributions.

mode of a graphene bilayer should have a vanishing $\gamma^{e\text{-ph}}$, since the bilayer bands are very similar to those of graphite with $k_\perp = 0$.

The temperature-dependent line shift is another quantity that is easily accessible by, e.g., Raman spectroscopy, and that provides powerful information on the anharmonicity. The ph-ph contribution to line shifts is given by the real part of the self-energy Π [22]; as mentioned before, at the lowest order this includes both 3-phonon and 4-phonon scattering terms. A further contribution descends straightforwardly from the lattice thermal expansion that is especially large and negative in graphene [17]. This contribution is obtained by computing the harmonic frequency at the lattice parameter appropriate to the given temperature, obtained within the quasiharmonic approximation [17]. Within the present approach the e-ph contribution to the frequency shift is taken into account exactly (within DFT) in the harmonic frequencies [18].

Figure 3 shows our computed line shifts for the E_{2g} mode [27]. The results are in good agreement with available experiments [28,29], and in excellent agreement with recent measurements for graphite and graphene [16]. In both cases the frequencies shift down with temperature—an unusual result for an optical mode where the bond-bond distances are predicted to become shorter with temperature. In reality, lattice contraction does provide the expected upward shift—and a much larger one for graphene than for graphite. Still, the overall behavior is dominated by a downshift driven by the 4-phonon scattering term, almost 2 times stronger in graphene than in graphite (Fig. 3). Thus, while the individual anharmonic contributions in graphite and graphene are quite different, the E_{2g} line shifts are always downward (driven by the 4-phonon contributions) and very similar in the two systems thanks to the compensation between different but opposite contributions.

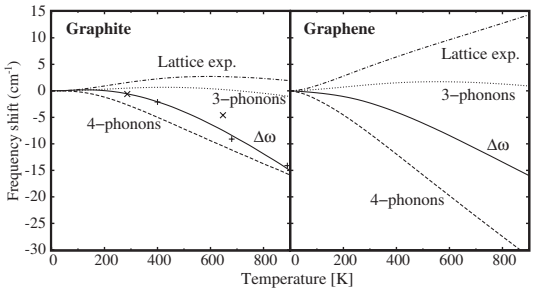

FIG. 3. Line shifts for the E_{2g} phonons in graphene and graphite: total shift $\Delta\omega$, solid lines (see footnote [31] for a polynomial fit to $\Delta\omega$); 3-phonon, 4-phonon, and thermal-expansion contributions, dotted, dashed, and dot-dashed lines, respectively. At 0 K, the 3-phonon and 4-phonon contributions for graphite (graphene) are -14.06 cm^{-1} and 1.30 cm^{-1} (-14.02 cm^{-1} and 3.03 cm^{-1}), respectively. Experimental data for graphite (+ , Ref. [28] and ×, Ref. [29]) are also shown.

Finally, we focus on the analysis of the anharmonic phonon decay processes. We show in Fig. 4 the anharmonic phonon lifetimes ($\tau = 1/\gamma^{\text{ph-ph}}$) and the decay channels for the modes E_{2g} at Γ and A_1' at K in graphene—these are the two modes with the strongest e-ph coupling, and the ones that will be overpopulated during steady-state operation in an interconnect [4] (the results for graphite are very similar; see Fig. 1). The values obtained are of the same

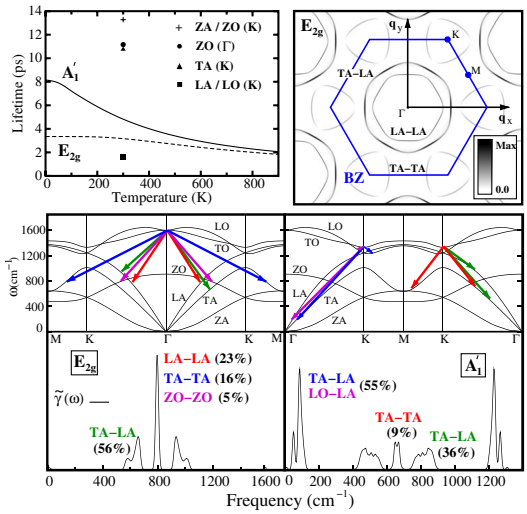

FIG. 4 (color online). Upper left panel: computed ph-ph lifetime of the E_{2g} and A_1' modes of graphene. We also report the computed lifetimes (300 K) of the other modes at Γ and K. Upper right panel: probability per unit time (300 K) that the E_{2g} mode at Γ decays into two phonons of wave vectors $\mathbf{q}$ and $-\mathbf{q}$. Upper part of the lower panel: schematic representation of the different ph-ph decay channels for the modes E_{2g} at Γ (left) and A_1' at K (right). Below, probability per unit time $\tilde{\gamma}$ that the E_{2g} or the A_1' modes (of frequency ω_0) decay into two modes of frequencies ω and ω_0-ω. The relative weight of the decay channels is also reported.

order of the optical-phonon thermalization time (7 ps) estimated in graphite from time-resolved terahertz spectroscopy [5]. This result is also in agreement with the empirical choice of Ref. [4] where the experimental I–V characteristic of metallic-tube interconnects was modeled by a coupled Boltzmann transport equation for phonons and electrons, assuming $\tau_\Gamma = \tau_K \sim 5$ ps. The values of τ_Γ and τ_K that we obtain from first-principles confirm this assumption, but provide much needed novel insight on the relative relevance of the different decay processes. In particular, it is found that $\tau_K > \tau_\Gamma$ (Fig. 4); in addition, since the e-ph coupling for the K mode is stronger than for Γ [4], we find that the phonon population at K will be dominant in determining inelastic losses, with the high-bias resistivity due to scattering with K phonons. Moreover, τ_K has a large decay channel toward low-energy acoustic phonon modes (Fig. 4, bottom right panel) that is not available to Γ phonons. This means that a strong temperature dependence is present in the typical operation range of 100–500 K, and that the population of acoustic phonons can strongly affect hot phonons and transport properties. Since acoustic phonons have a lower thermal-impedance mismatch with the substrate, it is expected that efficient thermalization strategies should focus on engineering the optimal coupling with the substrate. The present results and inclusion of acoustic phonons in the model of Ref. [4] should provide a realistic *ab initio* description of the coupled electronic and thermal dynamics in carbon nanostructures [30].

In conclusion, we have presented a detailed analysis of anharmonic effects in graphene and graphite, based on the explicit calculation of the ph-ph and e-ph interactions within DFPT. Excellent agreement with experimental results—where available—is found. We have explained the large differences in the linewidths for the closely related Raman and IR G bands in graphite, and the closely similar line shifts for the G band in graphene and graphite, notwithstanding very different thermal-expansion parameters. Moreover, the anomalous decrease of the Raman G band linewidth with temperature, predicted for both graphene and graphite, is rationalized through its dominant e-ph contribution; the negative dependence on temperature is accurately captured by a simple phenomenological expression. The ph-ph decay channels for the critical vibrational excitations that limit ballistic transport have been identified, with fundamental consequences in understanding and engineering electronic transport in metallic nanotubes and graphene ribbons interconnects.

We acknowledge support from the IFC Focus Center, a Semiconductor Research Corporation program, and MITRE (N. B.), and NSF No. DMR-0304019 (N. M.). Computational support was provided by IDRIS (Orsay, Project No. 071202), and NSF No. DMR-0414849 and PNNL No. EMSL-UP-9597.

[1] Z. Yao, C. L. Kane, and C. Dekker, Phys. Rev. Lett. **84**, 2941 (2000).
[2] M. Lazzeri *et al.*, Phys. Rev. Lett. **95**, 236802 (2005).
[3] E. Pop *et al.*, Phys. Rev. Lett. **95**, 155505 (2005).
[4] M. Lazzeri and F. Mauri, Phys. Rev. B **73**, 165419 (2006).
[5] T. Kampfrath *et al.*, Phys. Rev. Lett. **95**, 187403 (2005).
[6] L. Perfetti *et al.*, Phys. Rev. Lett. **96**, 027401 (2006).
[7] B. F. Habenicht *et al.*, Phys. Rev. Lett. **96**, 187401 (2006); Y. Miyamoto *et al.*, *ibid.* **97**, 126104 (2006); A. Gambetta *et al.*, Nature Phys. **2**, 515 (2006).
[8] J. Menendez and M. Cardona, Phys. Rev. B **29**, 2051 (1984).
[9] A. Shukla *et al.*, Phys. Rev. Lett. **90**, 095506 (2003).
[10] A. Debernardi *et al.*, Phys. Rev. Lett. **75**, 1819 (1995).
[11] R. A. Cowley, Rep. Prog. Phys. **31**, 123 (1968).
[12] S. Narasimhan and D. Vanderbilt, Phys. Rev. B **43**, 4541 (1991).
[13] J. Yan *et al.*, Phys. Rev. Lett. **98**, 166802 (2007). The spectral resolution of 2 cm^{-1} has been subtracted from the bare measurements.
[14] R. J. Nemanich *et al.*, Solid State Commun. **23**, 117 (1977).
[15] M. Lazzeri *et al.*, Phys. Rev. B **73**, 155426 (2006).
[16] A. C. Ferrari (private communication); I. Calizo *et al.*, arXiv:0708.1223v1.
[17] N. Mounet and N. Marzari, Phys. Rev. B **71**, 205214 (2005).
[18] S. Baroni *et al.*, Rev. Mod. Phys. **73**, 515 (2001).
[19] S. Baroni *et al.*, http://www.quantum-espresso.org.
[20] D. M. Ceperley and B. J. Alder, Phys. Rev. Lett. **45**, 566 (1980).
[21] N. Troullier and J. L. Martins, Phys. Rev. B **43**, 1993 (1991); M. Fuchs and M. Scheffler, Comput. Phys. Commun. **119**, 67 (1999).
[22] M. Lazzeri, M. Calandra, and F. Mauri, Phys. Rev. B **68**, 220509 (2003).
[23] M. Lazzeri and S. de Gironcoli, Phys. Rev. B **65**, 245402 (2002).
[24] S. Piscanec *et al.*, Phys. Rev. Lett. **93**, 185503 (2004).
[25] P. B. Allen, Phys. Rev. B **6**, 2577 (1972); P. B. Allen and R. Silberglitt, *ibid.* **9**, 4733 (1974).
[26] The $\mathbf{k}$-point sum in Eq. (1) is performed on a $2430 \times 2430 \times 144$ grid for graphite (and $2430 \times 2430 \times 1$ for graphene), using for δ a Lorentzian with a 0.13 mRy (20 K) width. To reduce the computational costs, this sum can be restricted to a small region around the K-H line where the addends are different from zero.
[27] The e-ph contribution changes by less than 1 cm^{-1} in the 0–800 K temperature range.
[28] H. Kagi *et al.*, Geochim. Cosmochim. Acta **58**, 3527 (1994).
[29] P. H. Tan *et al.*, Appl. Phys. Lett. **74**, 1818 (1999).
[30] N. Bonini *et al.* (to be published).
[31] A polynomial of the form $aT^2 + bT^3 + cT^4 + dT^5$ fits well (especially between 150–900 K) the *ab initio* results, with $a = 2.2679 \times 10^{-5}$, $b = -1.4836 \times 10^{-7}$, $c = 1.7869 \times 10^{-10}$, and $d = -7.1998 \times 10^{-14}$ for graphite and $a = -2.6595 \times 10^{-5}$, $b = -1.3568 \times 10^{-9}$, $c = 1.3633 \times 10^{-11}$, and $d = -4.0258 \times 10^{-15}$ for graphene.